Electronic Supplementary Material (ESI) for Physical Chemistry Chemical Physics.

SUPPORTING INFORMATION

Exciton Delocalization in a Fully Synthetic DNA-Templated Bacteriochlorin Dimer

Olga A. Mass,[1,*] Devan R. Watt,[1] Lance K. Patten,[1] Ryan D. Pensack,[1] Jeunghoon Lee,[1,3] Daniel B. Turner,[1] Bernard Yurke,[1,2] and William B. Knowlton. [1,2]

[1]Micron School of Materials Science & Engineering, [2]Department of Electrical & Computer Engineering, [3]Department of Chemistry and Biochemistry, Boise State University, Boise, Idaho 83725, United States

Corresponding author:

*olgamass@boisestate.edu

Table of Contents

S1	^{1}H and ^{13}C NMR Spectra	S2
S2	Oligo Sequences	S8
S3	Electrophoretic Analysis	S10
S4	Absorption Spectra of “Free” Bacteriochlorins	S11
S5	Fluorescence Spectra	S12
S6	Full Absorption and Circular Dichroism Spectra of **BC** Monomer and Dimer HJ Constructs	S13
S7	Digitizing Procedure of **Bchl*a*** Spectral Data	S15
S8	Kühn-Renger-May Modeling	S17
S9	References	S29

Supporting Information 1: *[1]H and [13]C NMR Spectra*

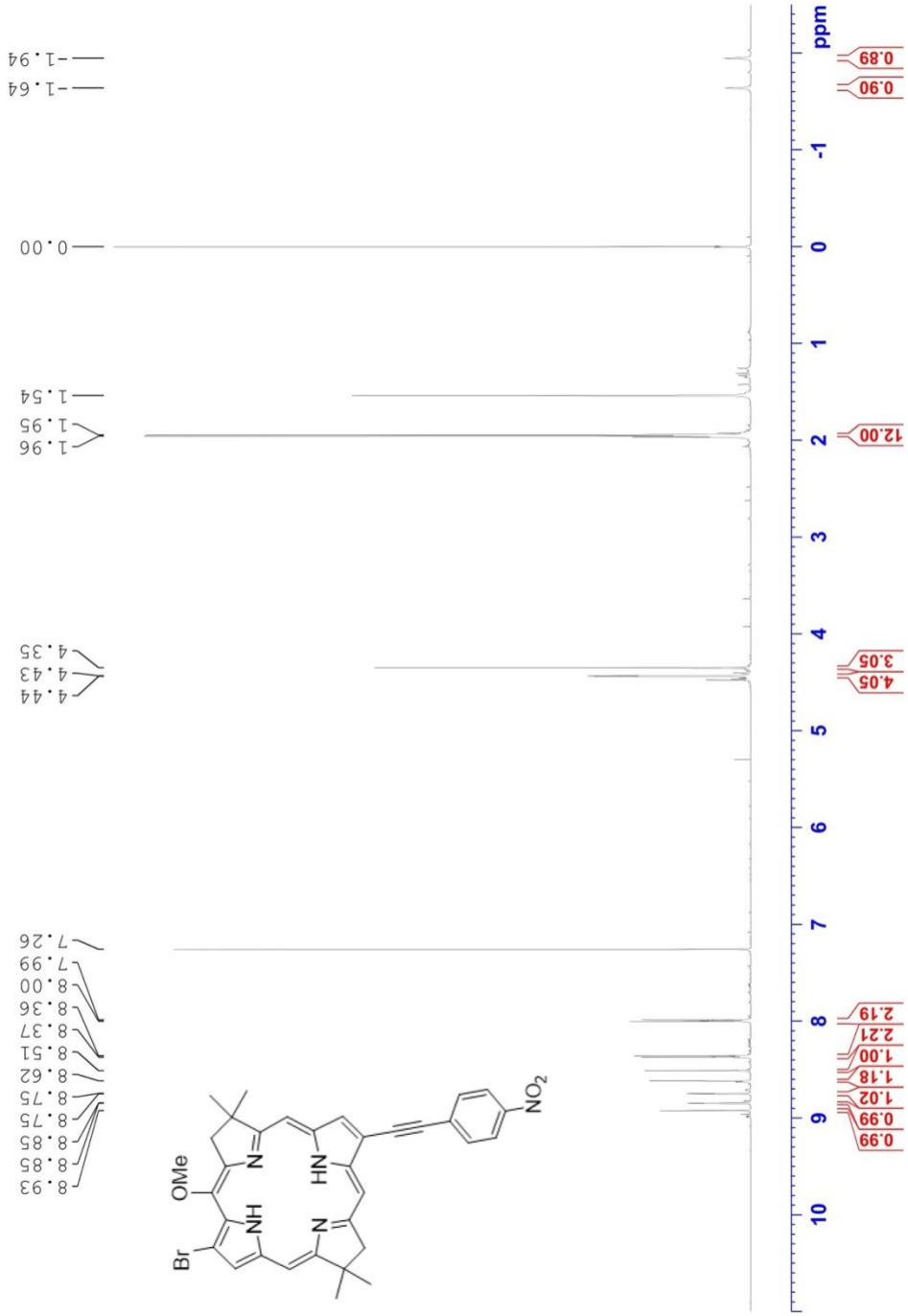

Figure S1: [1]H NMR spectrum of **3** ($CDCl_3$, 600 MHz).

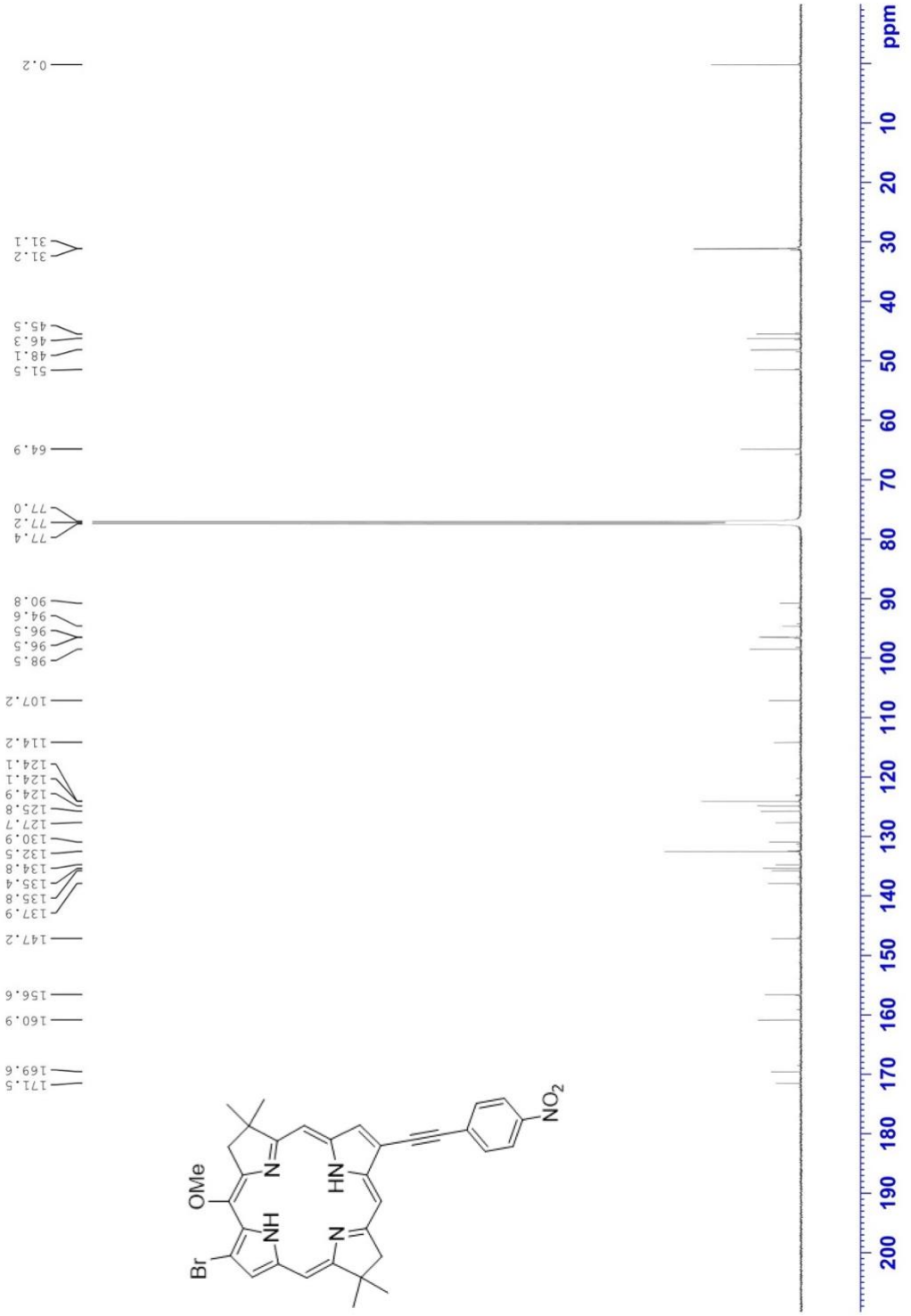

Figure S2: ^{13}C NMR spectrum of **3** ($CDCl_3$, 600 MHz).

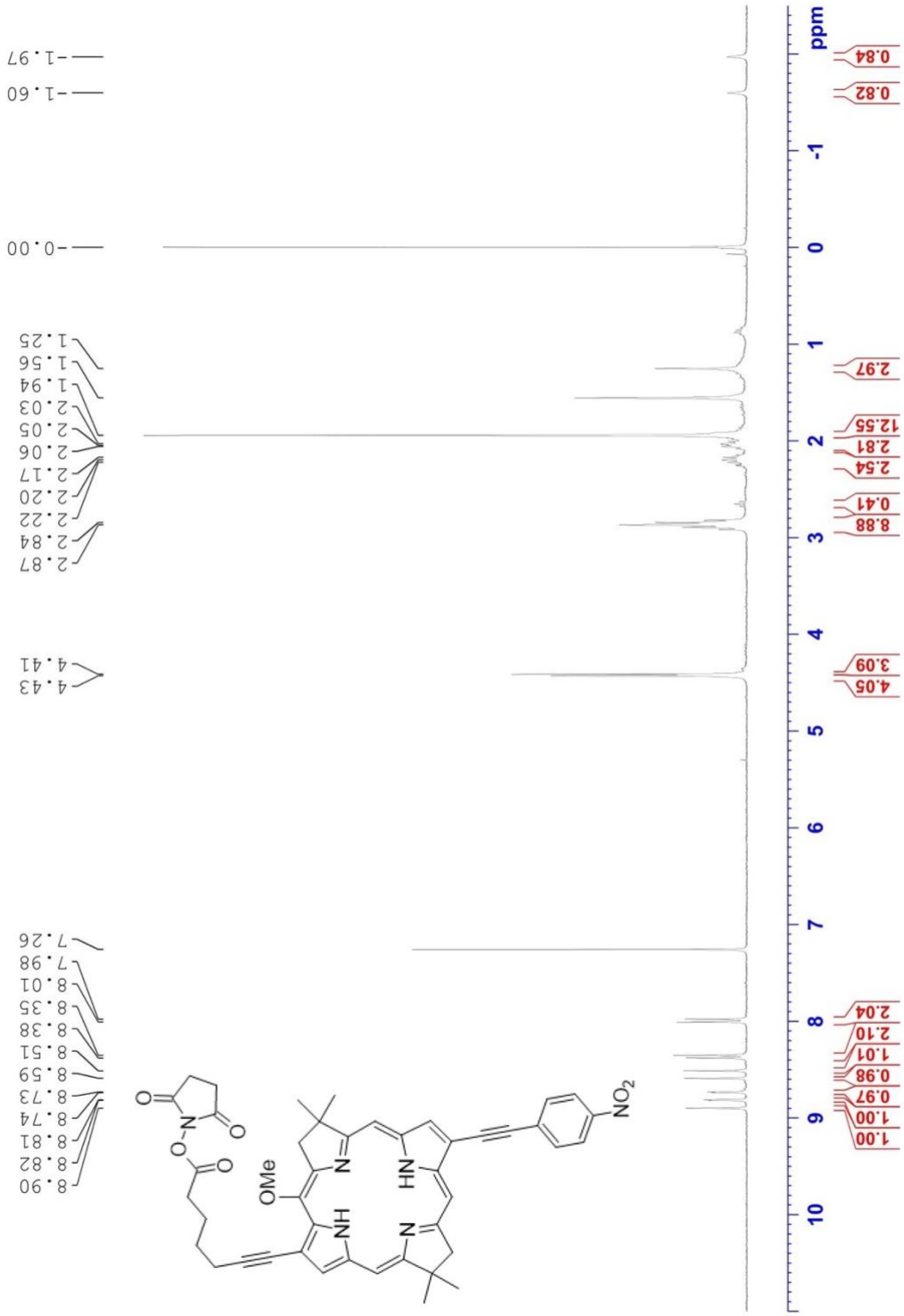

Figure S3: ^{1}H NMR spectrum of **BC** ($CDCl_3$, 600 MHz).

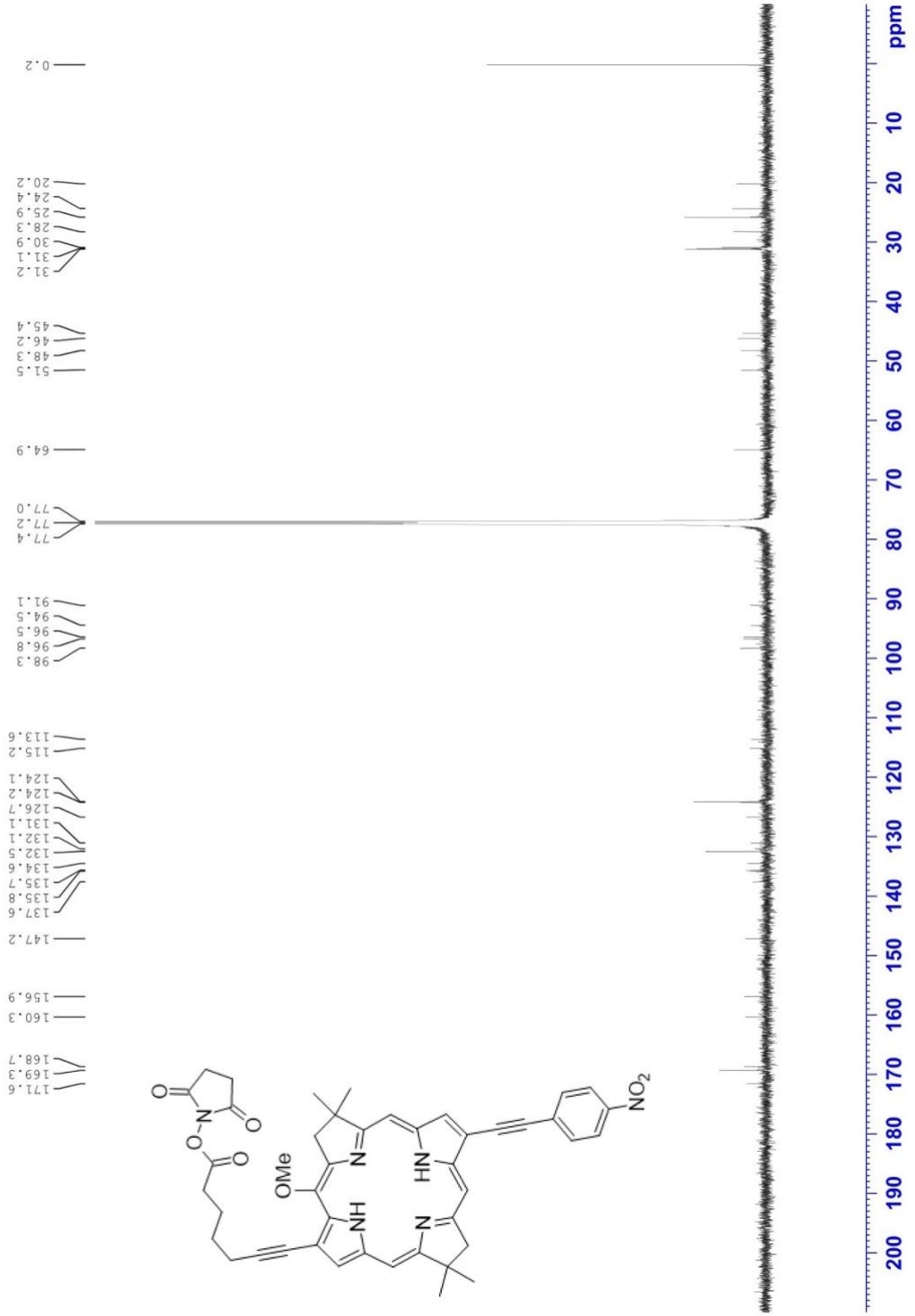

Figure S4. ^{13}C NMR spectrum of **BC** ($CDCl_3$, 600 MHz).

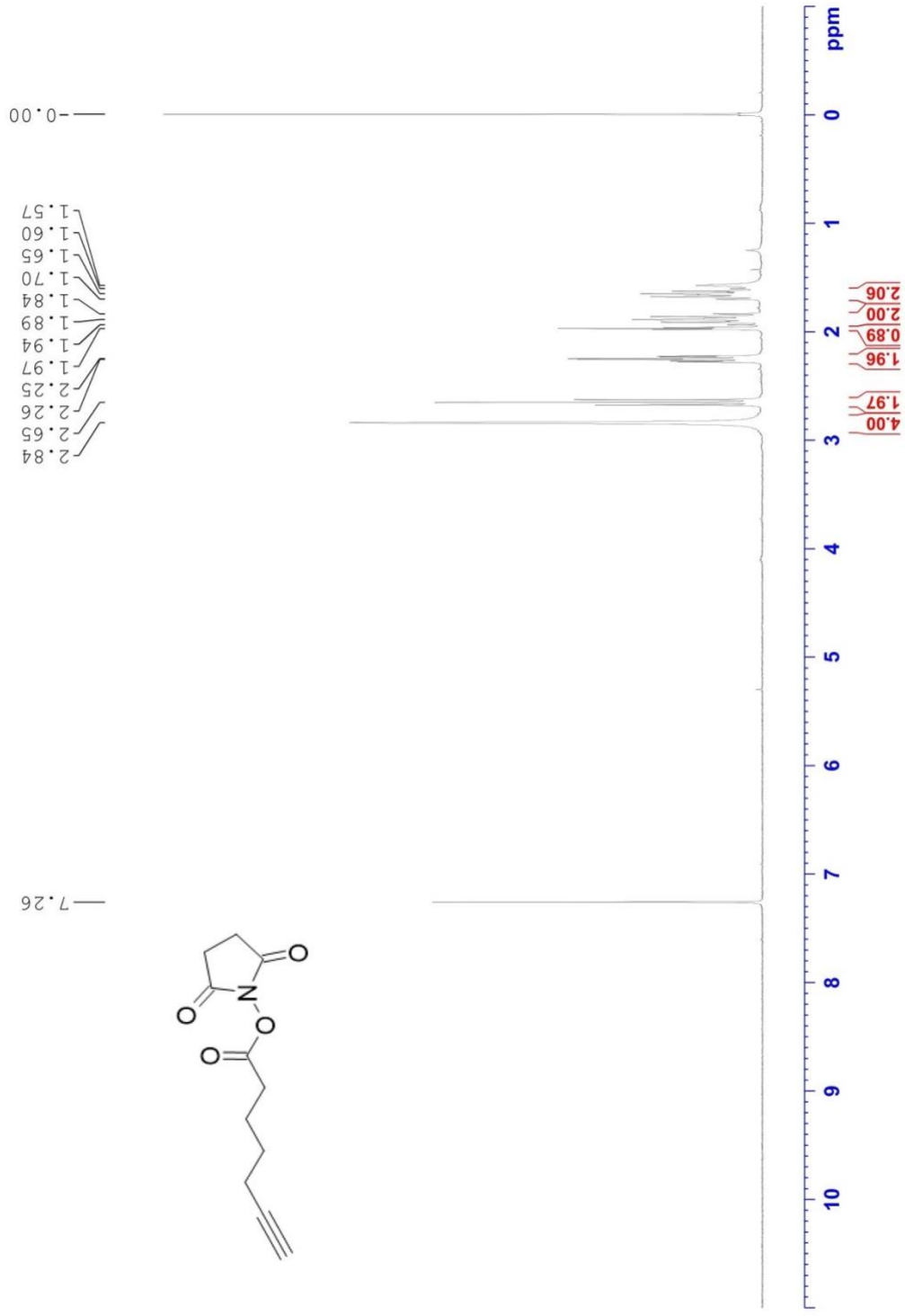

Figure S5: ^{1}H NMR spectrum of **4** ($CDCl_3$, 300 MHz).

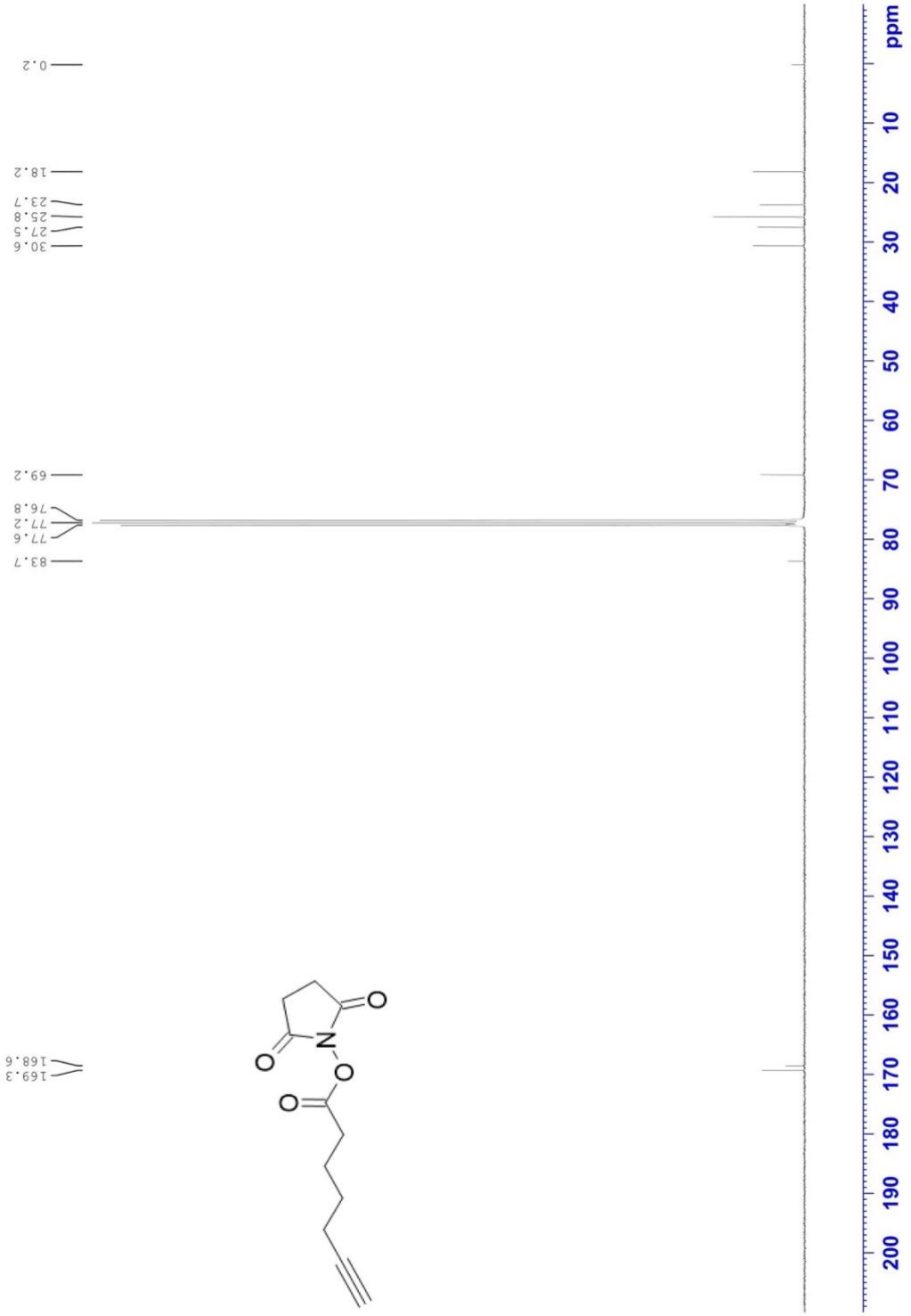

Figure S6: ^{13}C NMR spectrum of **4** ($CDCl_3$, 300 MHz).

Supporting Information 2: *Oligo Sequences*

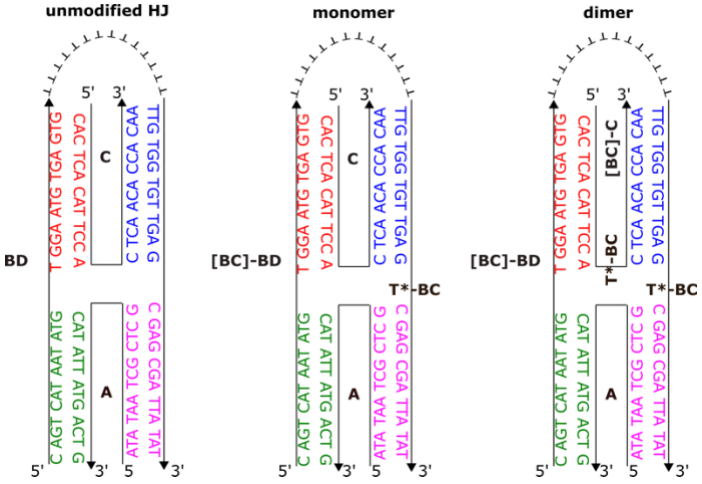

Table S1. Oligo sequences used to assemble bacteriochlorin monomer and dimer Holliday junction constructs.

Strand Name	[a]Sequence (5' to 3')	Length (nt)	Purification
A	ATATAATCGCTCGCATATTATGACTG	26	desalting
C	CACTCACATTCCACTCAACACCACAA	26	desalting
BD	CAGTCATAATATGTGGAATGTGAGTGTTTTTTTTTTTTT TTGTGGTGTTGAGCGAGCGATTATAT	66	desalting
[BC]-C	CACTCACATTCCA[T*-BC]CTCAACACCACAA	27	HPLC
[BC]-BD	CAGTCATAATATGTGGAATGTGAGTGTTTTTTTTTTTTT TTGTGGTGTTGAG[T*-BC]CGAGCGATTATAT	67	HPLC

[a]complementary sequence regions are color-coded.

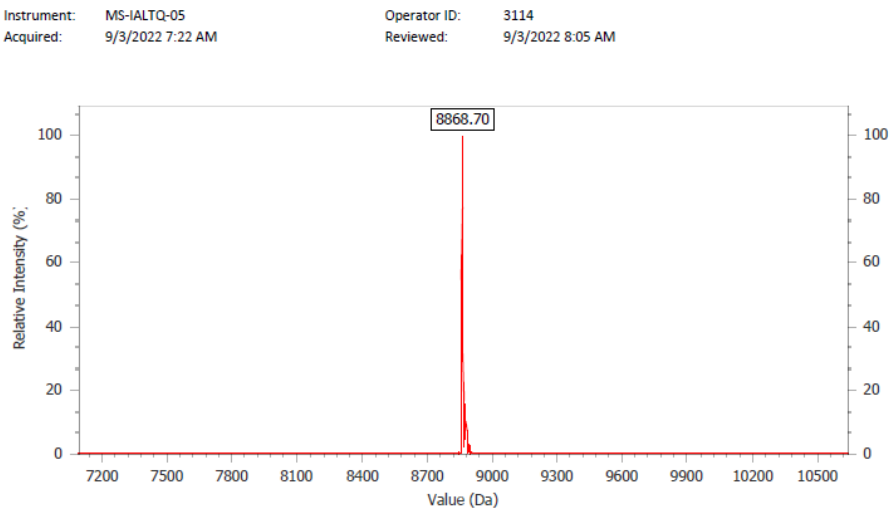

Sequence Name: C(BC5)
Sequence: 5'- CAC TCA CAT TCC A/iNonCat097/C TCA ACA CCA CAA -3'
Calculated Molecular Weight: 8867.3
Measured Molecular Weight: 8868.70

Figure S7: Analytical ESI-MS spectrum of BC-labeled oligo strand [BC]-C.

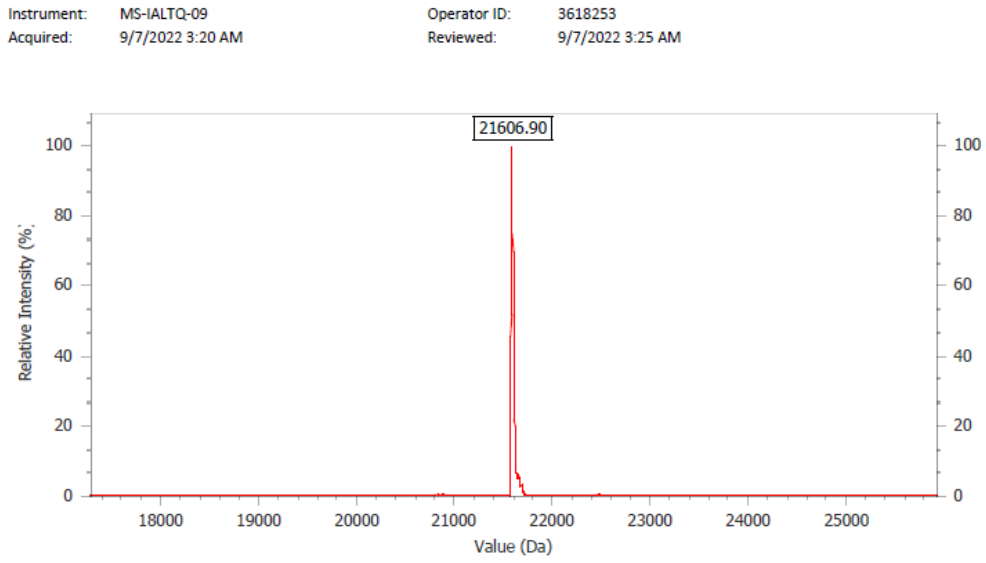

Sequence Name: B(BC5)/D T14
Sequence: 5'- CAG TCA TAA TAT GTG GAA TGT GAG TGT TTT TTT TTT TTT TTT GTG GTG TTG AG/iNonCat097/ CGA GCG ATT ATA T -3'
Calculated Molecular Weight: 21607.5
Measured Molecular Weight: 21606.90

Figure S8: Analytical ESI-MS spectrum of BC-labeled oligo strand [BC]-BD.

Supporting Information 3: *Electrophoresis*

Non-denaturing polyacrylamide gel electrophoresis (PAGE) was carried out to confirm the formation of bacteriochlorin-HJ construct after hybridization. The 15% non-denaturing electrophoresis gel, 1.5 mm was casted in 1× TBE 15 mM $MgCl_2$. DNA samples were diluted 10-fold in Loading Buffer (Ficoll (SigmaAldrich) 20% v/v, bromophenol blue (SigmaAldrich) 20% v/v. The DNA HJ samples and control single strands were loaded on the gel at the final DNA concentration 0.15 μM (Gel 1). The gel was run for 2 h 35 min at 150 V constant voltage at 17 °C constant temperature in running buffer 1× TBE, 15 mM $MgCl_2$. The electrophoresed gel was treated with SYBR Gold (Invitrogen) for 30 min and imaged using FluorChem Q imager (Alpha Innotech) under the Cy2-channel (ex. 475 nm, em. 537 nm). The resulting raw image and contrast-adjusted image are shown in **Fig. S9ab**. The dimer construct was poorly detectable, presumably due to the overlap of Cy2 emission and BC absorption. As such, Gel 2 with sample concentrations of 0.35 μM was developed under identical conditions to detect dimer construct (**Fig. S9cd**).

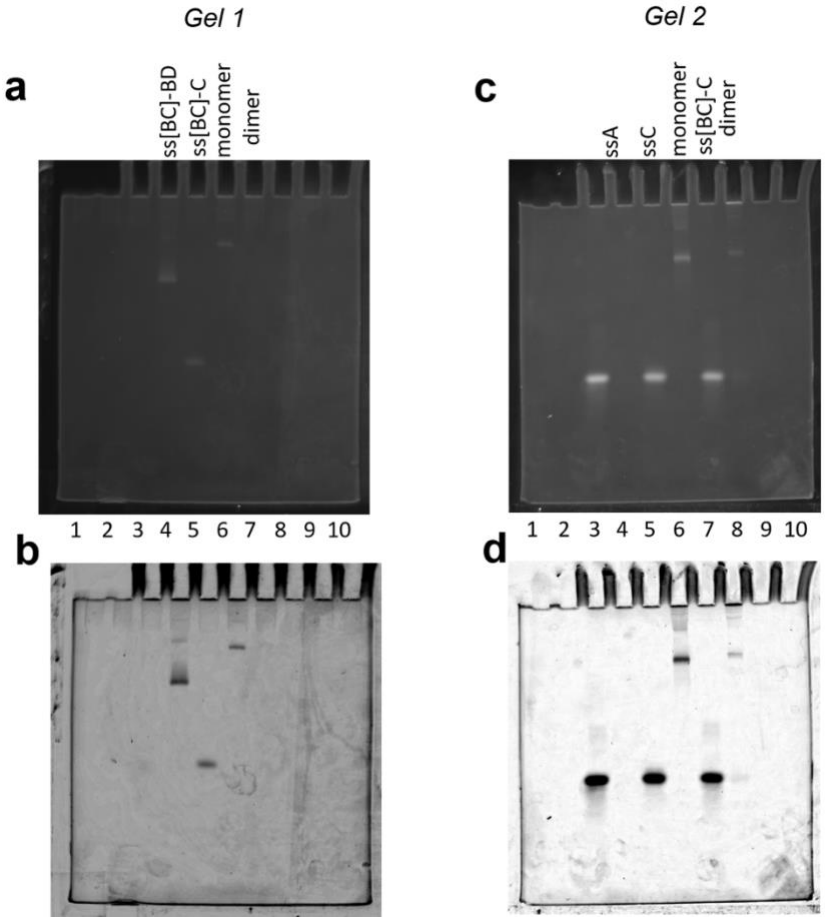

Figure S9. Fluorescence image (ex. 475 nm, em. 537 nm) of SYBR Gold-stained non-denaturing PAGE (15%) of bacteriochlorin-HJ constructs. (**a**) raw image of Gel 1: lane 4 – [BC]-BD single strand; lane 5 – [BC]-C single strand; lane 6 – monomer; lane 7 – dimer; lanes 1-3 and 8-10 – empty. (**b**) contrast-adjusted image of Gel 1. (**c**) raw image of Gel 2: lane 3 – A single strand; lane 5 – C single strand; lane 6 – monomer; lane 7 – [BC]-C single strand; lane 8 - dimer; lanes 1, 2, 4, and 9-10 - empty. (**d**) contrast-adjusted image of Gel 2.

Supporting Information 4: *Absorption Spectra of "Free" Bacteriochlorins*

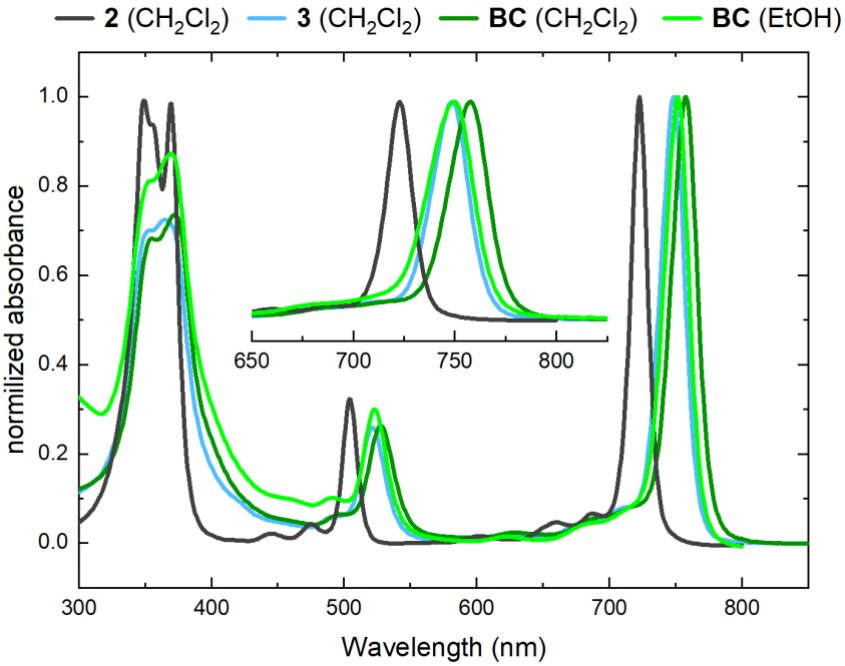

Figure S10. Steady-state absorption of bacteriochlorins **2**, **3**, and **BC** normalized at the $Q_y(0,0)$ absorption band maxima. The inset shows a magnification of the Q_y region. The measurements were recorded at room temperature.

Table S2. Absorption characteristics of bacteriochlorins **2**, **3,** and **BC**.

"Free" Dye	solvent	λ $B_y(0,0)$, $B_x(0,0)$/ nm	λ $Q_x(0,0)$/ nm	λ $Q_y(0,0)$/ nm
2	dichloromethane	349, 370	504	723
3	dichloromethane	355, 365	521	749
BC	dichloromethane	355, 373	528	758
BC	ethanol	353, 369	522	750

Supporting Information 5: *Fluorescence Spectra*

Steady-state fluorescence spectra were recorded at room temperature using a Horiba PTI QuantaMaster 400 spectrofluorometer (Horiba Scientific) in a 1 cm path length quartz cuvette (Starna) and monitored as a function of wavelength when excited at λ_{exc} = 530 nm. The fluorescence spectra were scaled by the absorptance at the excitation maximum. The absorptance is defined as

$$A = 1 - T = 1 - 10^{-abs}$$

where A is absorptance at the excitation wavelength (λ_{exc}), T – transmitted light, and abs – absorption at $\lambda_{exc.}$

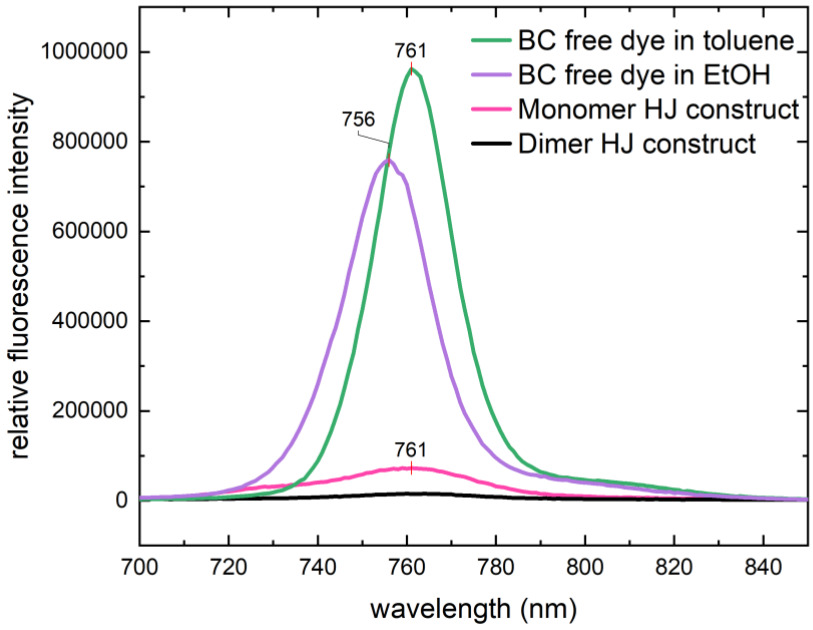

Figure S11. Relative fluorescence intensities of "free" **BC** in toluene and ethanol and **BC** monomer and dimer HJ constructs in 1× TBE, 15 mM $MgCl_2$. The concentration of **BC** monomer HJ and dimer HJ were 4.0 μM. The spectra were recorded at room temperature. The samples were excited at λ_{exc} = 530 nm. The fluorescence was scaled by the absorptance at the excitation wavelength.

Supporting Information 6: *Full Absorption and Circular Dichroism Spectra of **BC** Monomer and Dimer HJ Constructs*

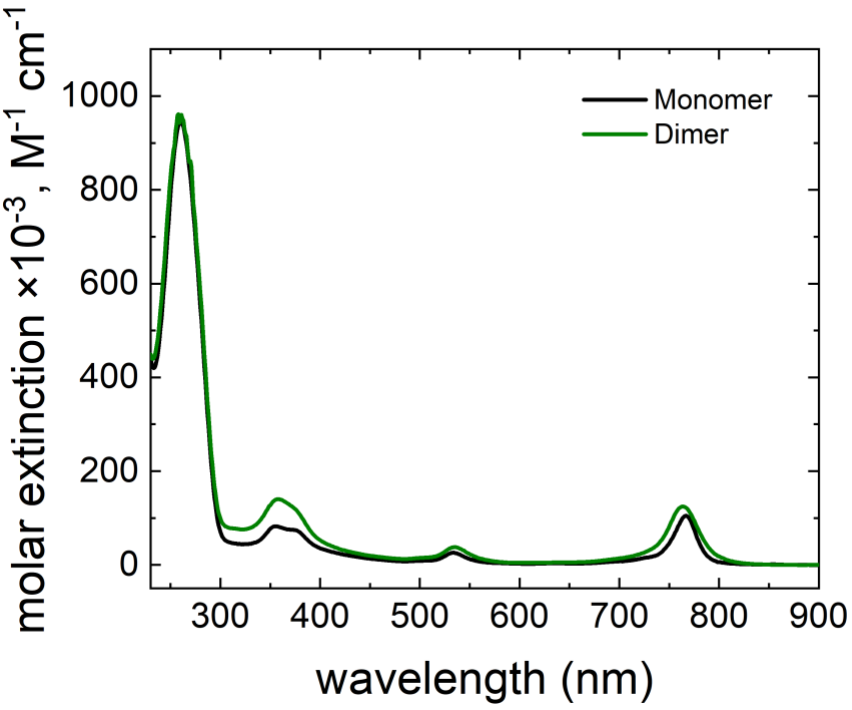

Figure S12. Acquired steady-state absorption spectra converted to extinction of BC monomer and dimer HJ constructs. The spectra were recorded at room temperature. The monomer and dimer sample concentrations were 1.5 μM in 1× TBE, 15 mM $MgCl_2$.

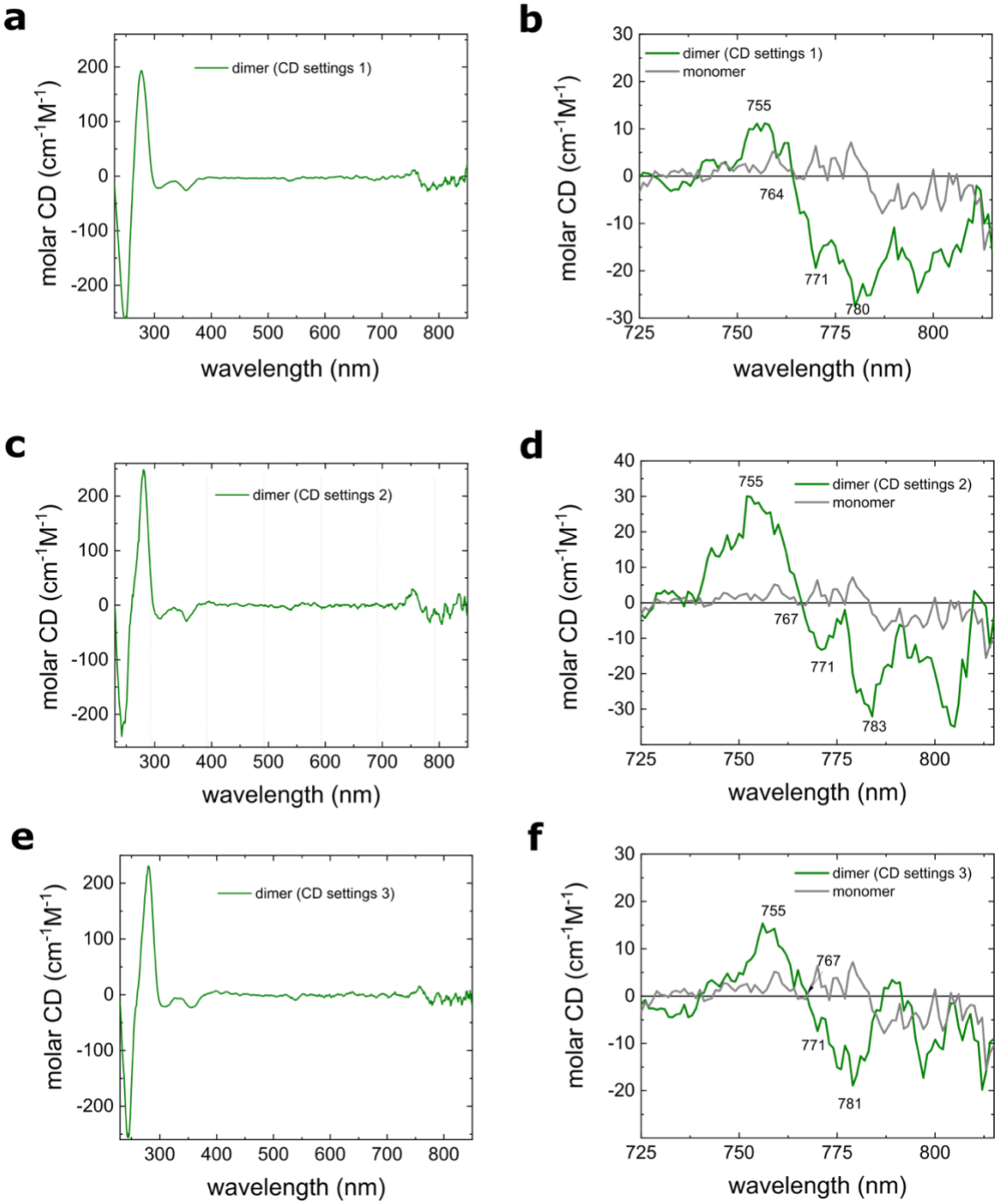

Figure S13. Acquired steady-state circular dichroism spectra of **BC** monomer and dimer HJ constructs at 4.0 μM in 1× TBE, 15 mM $MgCl_2$ at room temperature in 120 μL cuvette and several CD settings: (**a,b**) 100 nm/min, 4 s data integration time (DIT), 2 nm bandwidth, 3 accumulations; (**c,d**) 200 nm/min, 2 s DIT, 1 nm bandwidth, 3 accumulations, and (**e,f**) 200 nm/min, 2 s DIT, 1 nm bandwidth, 9 accumulations.

Supporting Information 7: *Digitizing Procedure of **Bchla** Spectral Data*

For the KRM modeling, the absorbance and circular dichroism spectral data of **Bchl*a*** "free" dye and dimer were obtained from the publication of Parkes-Loach et al.[1] In that study, the **Bchl*a*** dimer templated by LH1 α/β apoprotein referred as **820B** was isolated from *R. rubrum* with the removal of carotenoid and ubiquinone.[1] The free **Bchl*a*** referred as **777B** was obtained by dissociation of **820B**. [1]The absorbance of **820B** was reported to be recorded at about 10 μM.[1] We extracted the datapoints of the relative absorption and CD spectra from [1] using WebPlotDigitizer 4.6.[2] The relative absorbance was converted into molar extinction applying Beer's law and using the reported extinction coefficients of 80.6 $mM^{-1}\cdot cm^{-1}$ and 61.7 $mM^{-1}\cdot cm^{-1}$, for **820B** and **777B** respectively[3]. The resulting digitized spectra are shown in **Fig. S14**. The digitizing procedure was validated by calculation of sample concentrations using the above extinction coefficients, and relative absorption peak maxima from the digitized absorption plot to afford 10.0 μM. The circular dichroism spectrum of **820B** was digitized in the same manner and converted into units of molar CD using **820B** concentration of 10.0 μM (**Fig. S15**).

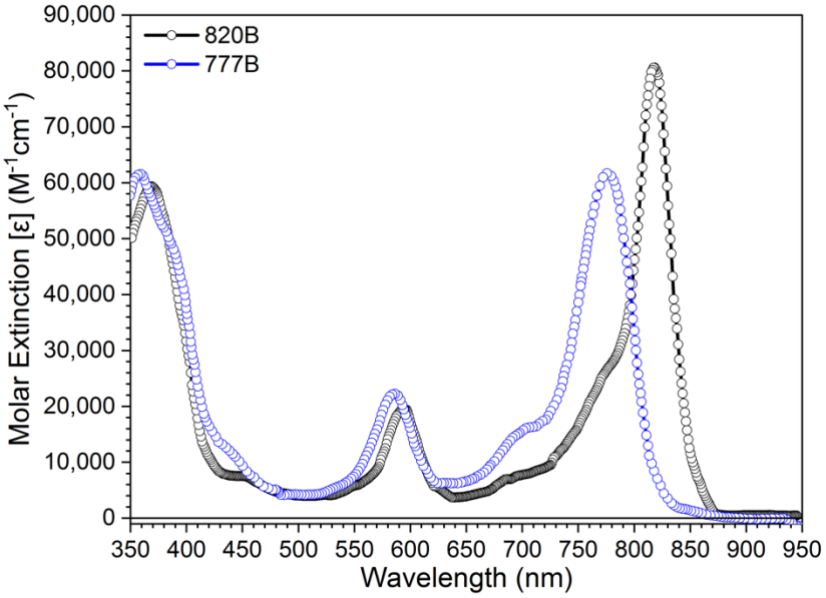

Figure S14. The absorption spectra of **777B** single dye and **820B** dimer digitized from ref. [1] and converted into molar extinction. The relative absorption of **820B** was reported to be recorded in phosphate buffer containing 0.72% *n*-octyl *β*-D-glucopyranoside. The relative absorption of **777B** was reported to be recorded by adding a methanol solution of **Bchl*a*** to phosphate buffer containing 4.5% *n*-octyl *β*-D-glucopyranoside.

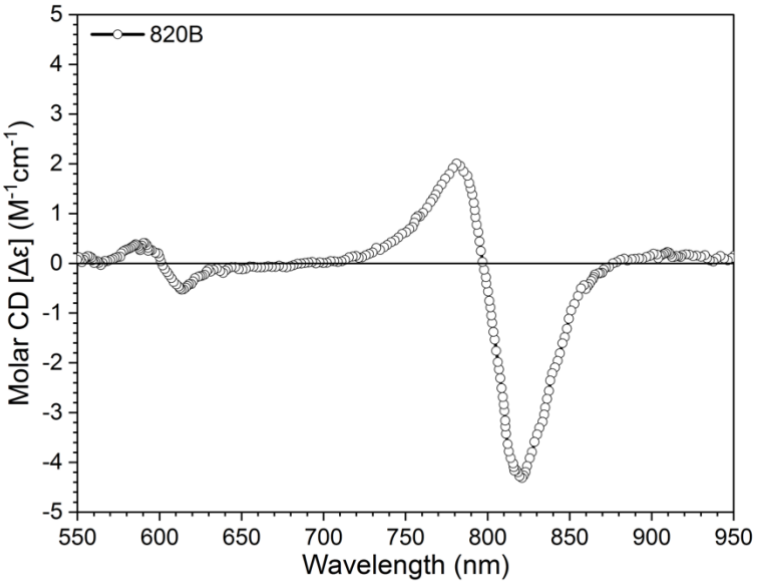

Figure S15. The circular dichroism of **820B** digitized from ref. [1] and converted into molar CD. The circular dichroism of **820B** was reported to be recorded at 10 μM concentration in phosphate buffer supplemented with *n*-octyl *β*-D-glucopyranoside.

Supporting Information 8: *Kühn-Renger-May Modeling*

The modeling based on Kühn-Renger-May approach (KRM)was performed following the established modeling procedure described in detail by Roy et al.[4]

Molecular (Frenkel) exciton behavior is well approximated by a Holstein-like[5] augmented Frenkel Hamiltonian[6] of the form:

$$\hat{H} = \hat{H}^{(e)} + \hat{H}^{(v)} \qquad \text{(eq S1)}$$

The KRM Model Simulation tool considers the case of single excitations. Terms involving double excitations are omitted to give the electronic part of the Hamiltonian as:

$$\hat{H}^{(e)} = \sum_{m} \varepsilon_m^e \hat{B}_m^\dagger \hat{B}_m + \sum_{m,n}^{m \neq n} J_{m,n} \hat{B}_m^\dagger \hat{B}_n \qquad \text{(eq S2)}$$

where ε_m^e is the monomer transition energy, $J_{m,n}$ is the excitonic hopping parameter associated with transition dipole coupling between chromophores m and n from a single exciton, and the operators $\hat{B}_i^\dagger$ and $\hat{B}_i$ are exciton creation and annihilation operators, respectively.

The excitonic hopping parameter $J_{m,n}$ is often expressed in a point dipole-dipole interaction form[6-8] representing the interaction between a pair of molecular transition dipoles μ_m and μ_n for the dyes at sites *m* and *n*:

$$J_{m,n} = \frac{1}{4\pi\varepsilon\varepsilon_0}\left(\frac{\boldsymbol{\mu_m} \cdot \boldsymbol{\mu_n}}{\left|\boldsymbol{R_{m,n}}\right|^3} - \frac{(\boldsymbol{\mu_m} \cdot \boldsymbol{R_{m,n}})(\boldsymbol{\mu_n} \cdot \boldsymbol{R_{m,n}})}{\left|\boldsymbol{R_{m,n}}\right|^5}\right) \qquad \text{(eq S3)}$$

where $\boldsymbol{R_{m,n}}$ – the position vector between the dye centers of dyes *m* and *n* (further $\boldsymbol{R_{1,2}}$ between two dyes).

However, to better account for the physical charge distribution that spreads out over the length of the molecule, the extended dipole approximation was utilized. In the extended dipole approximation,[9] the Coulomb energy between a pair of dipoles is given in Standard International units by:

$$J_{m,n} = \frac{\delta^2}{4\pi\epsilon_0\epsilon_r}\left(\frac{1}{|\boldsymbol{r_1}-\boldsymbol{r_2}|} - \frac{1}{|\boldsymbol{r_1}-\boldsymbol{s_2}|} - \frac{1}{|\boldsymbol{s_1}-\boldsymbol{r_2}|} + \frac{1}{|\boldsymbol{s_1}-\boldsymbol{s_2}|}\right) \qquad \text{(eq S4)}$$

where δ is the oscillating point charge in Coulombs, ϵ_0 is the permittivity of the vacuum ($\epsilon_0 = 8.85 \times 10^{-12}\ \frac{A^2 s^4}{m^3 kg}$), ϵ_r is the relative dielectric constant of the medium, $\boldsymbol{r_1}$ and $\boldsymbol{s_1}$ are the

location of the "+" and "- "charges on molecule *1* and similarly for molecule *2*. The distance units are meters and the exchange energy $J_{m,n}$ unit is in electron volts.

The transition dipole moment is given by $\mu = \delta l$ where l is the distance in meters between the two point charges on a given molecule, and *r* is given by $\epsilon_r = n^2$ where *n* is the index of refraction of the medium.

The transition dipole moment was determined using the following equation:[10]

$$M_{01} = 9.58 \times 10^{-2} \left(\frac{\left(2n^2+1\right)^2}{9n^3} \int \frac{\epsilon(\nu)}{\nu} d\nu \right)^{\frac{1}{2}} \quad \text{(eq S5)}$$

M_{01} – transition dipole moment in debye; *n* - refractive index of water (n_{water} = 1.3327).

Note that μ has units of Coulomb meters while M_{01} has units of debye. The conversion relation between the two is 1 debye = 3.33564×10^{30} C·m.

Then the equation (S4) can be rewritten as:

$$J_{12} = \frac{J_0}{l^2} \left(\frac{1}{|\boldsymbol{r_1}-\boldsymbol{r_2}|} - \frac{1}{|\boldsymbol{r_1}-\boldsymbol{s_2}|} - \frac{1}{|\boldsymbol{s_1}-\boldsymbol{r_2}|} + \frac{1}{|\boldsymbol{s_1}-\boldsymbol{s_2}|} \right) \quad \text{(eq S6)}$$

Where characteristic excitonic hopping paramter $J_0 = \frac{\mu^2}{4\pi\epsilon_0 n^2}$ (eq S7)

The quantity J_0 has units of J·m^3.

When the position vectors $\boldsymbol{r}$ and $\boldsymbol{s}$ are rewritten as:

$$\boldsymbol{r_1} = \boldsymbol{R_1} + \frac{l}{2}\boldsymbol{n_1} \qquad \boldsymbol{s_1} = \boldsymbol{R_1} - \frac{l}{2}\boldsymbol{n_1} \qquad \boldsymbol{r_2} = \boldsymbol{R_2} + \frac{l}{2}\boldsymbol{n_2} \qquad \boldsymbol{s_2} = \boldsymbol{R_2} - \frac{l}{2}\boldsymbol{n_2}$$

And when $|\boldsymbol{R_1} - \boldsymbol{R_2}| \gg l$, equation (eq S6) reduces to:

$$J_{12} = \frac{J_0}{|\boldsymbol{R_1}-\boldsymbol{R_2}|^3} [\boldsymbol{n_1} \cdot \boldsymbol{n_2} - 3(\boldsymbol{n_{12}} \cdot \boldsymbol{n_1})(\boldsymbol{n_{12}} \cdot \boldsymbol{n_2})] \quad \text{(eq S8)}$$

where $\boldsymbol{n_{12}} = \frac{\boldsymbol{R_1}-\boldsymbol{R_2}}{|\boldsymbol{R_1}-\boldsymbol{R_2}|}$

Thus, J_0 is the same constant in both the point dipole-dipole approximation and in the extended dipole approximation.

In addition to the electronic components described above, the KRM Model Simulation Tool considers coupling with up to two vibrational quanta. The exciton-vibron coupling Hamiltonian can be written as:

$$\hat{H}^{(v)} = \sum_m \sum_\alpha \varepsilon_m^v \hat{A}_{m,\alpha}^\dagger \hat{A}_{m,\alpha} + \sum_m \sum_\alpha D_{m,\alpha} \hat{B}_m^\dagger \hat{B}_m \left(\hat{A}_{m,\alpha}^\dagger + \hat{A}_{m,\alpha}\right)$$

(eq S9)

where ε_m^v is the energy spacing between vibrational levels, $D_{m,\alpha}$ is related to the displacement of the harmonic oscillator potential of the excited state from the electronic ground state minimum , and $\hat{A}_{m,\alpha}^\dagger$ and $\hat{A}_{m,\alpha}$ are the vibron creation and annihilation operators for chromophore *m* and vibrational mode α. Vibrational energy spacing and displacement are determined using experimental data from the relevant monomer.

The theoretical absorbance as a function of energy, for comparison with experimental data, was computed from the line spectra obtained by diagonalizing the system Holstein-like Hamiltonian[5] by convolution with a Gaussian as:

$$A(E) = \sum_i \frac{\gamma_i}{\sqrt{2\pi\Gamma^2}} exp\ \left(-\frac{(E-E_i)^2}{2\Gamma^2}\right) \quad \text{(eq S10)}$$

Where the γ_i is the transition rate between the ground state E and the state having the eigenenergy E_i, and Γ is a linewidth.

Similarly, the CD absorbance as a function of energy was computed as:

$$A_{CD}(E) = \sum_i \frac{\gamma_i^{CD}}{\sqrt{2\pi\Gamma^2}} exp\left(-\frac{(E-E_i)^2}{2\Gamma^2}\right) \quad \text{(eq S11)}$$

The phenomenological constants used for fitting the monomer and dimers data in the theoretical model are shown in Table S3. Appling extended dipole-dipole approximation, we used the TDM length defined as a distance between point charges of opposite sign. We tested three placement of point charges and, hence, three TDM lengths measured using the Avogadro software (v.1.2.0): 0.9 nm (between pyrrolic β-carbons), 1.0 nm (between alkyne carbons adjacent to the macrocycle), and 1.15 nm (between the centers of the triple bonds). The variation in the point charge placement and TDM length did not affect the final *J* value and had a negligible effect on the angular orientation of the TDMs. As such, we report the modeling results for the 1.15 nm corresponding to the length of TDM between the centers of the triple bonds. The linewidth Γ to be 0.028-0.034 eV, and the number of vibronic states n_v to be 3 (**Table S4**).

The values of characteristic exciton hopping parameter J_0 calculated from M_{01} according to the equation (S7) are reported in **Table S3**, and its values were used as a fitting parameter in the calculations of **BC** and **Bchl*a*** dimers.

Stochastic Gradient Descent Search

To facilitate an efficient search of the unique configuration, each set of generated spectra is given a fitness score for comparison with the following iterations. At each iteration, TDM mutual orientation is arbitrarily alternated with the proximity limited to cdis of 0.34 nm between any two points. After each alternation, new theoretical absorption and CD spectra are computed, and their fitness scores are compared to the spectra in the previous iteration. The program selects the better fitness score, retains the corresponding TDM orientation, and proceeds to the next iteration. Upon completion, the program outputs the results derived from the best-observed match between experimental and theoretical spectra.

Initial TDM Orientations

To ensure the unique solution of each spectral fitting, the modeling of each dimer was performed in duplicates starting by placing the TDMs 2 nm apart in two extreme initial orientations: an end-to-end and face-to-face. Both starting orientations afforded the same outcomes for each dimer.

Goodness of Fit

As a measure of the goodness of fit, we evaluated the overlap integrals of the experimental spectra with the theoretical spectra (**Table S5**). Letting $\int S_{ab,ex}(E), S_{ab,th}(E)$, $S_{cd,ex}(E), and\ S_{cd,th}(E)$ denote respectively the experimental absorbance spectrum, theoretical absorbance spectrum, experimental CD spectrum, and theoretical CD spectrum where ***E*** is energy, the normalized absorbance overlap integral OI_{AB} of the spectrum is defined by:

$$OI_{AB} = \frac{\int S_{ab,ex}(E) S_{ab,th}(E) dE}{\sqrt{\int S_{ab,ex}^2(E) dE}\sqrt{\int S_{ab,th}^2(E) dE}} \quad \text{(eq S12)}$$

and the normalized overlap integral for the CD spectrum OI_{CD} is defined by:

$$OI_{CD} = \frac{\int S_{cd,ex}(E) S_{cd,th}(E) dE}{\sqrt{\int S_{cd,ex}^2(E) dE}\sqrt{\int S_{cd,th}^2(E) dE}} \quad \text{(eq S13)}$$

As an overall goodness parameter, we introduce:

$$OI_{tot} = \frac{1}{2}(OI_{ab} + OI_{cd}) \quad \text{(eq S14)}$$

In addition, the mean-square deviation of absorbance and CD were utilized:

$$ms_{abs} = \sum_i [S_{ab,ex}(E) - S_{ab,th}(E)]^2 \quad \text{(eq S15)}$$

$$ms_{cd} = \sum_i [S_{cd,ex}(E) - S_{cd,th}(E)]^2 \quad \text{(eq S16)}$$

$$Fitness = w_1(1-r)^2 + w_2(1-OI_{AB})^2 + w_3(1-OI_{CD})^2 + w_4 ms_{abs} + w_5 ms_{cd} \quad \text{(eq S17)}$$

where w_1, w_2, w_3, and w_4 are user selected weights. For a typical run, the weights were chosen as $w_1 = 1$, $w_2 = w_3 = 0$, and $w_4 = w_5 = 1$.

Aggregate Geometry

The resulting outputs of the fit provide information regarding the angles and position of the dye transition dipole moments relative to each other. Spherical coordinates, the zenith (θ_i) and azimuth (φ_i) angles, are given in degrees. The Cartesian components of the orientation vector for a dye are given in terms of θ_i and φ_i by the following set of equations:

$$n_x = sin\ (\theta_i)\ cos\ (\varphi_i)$$

$$n_y = sin\ (\theta_i) \sin(\varphi_i)$$

$$n_z = cos\ (\theta_i)$$

The positions of the dyes are given in nm and listed in **Table S6.**

A center-to-center distance R between two dyes was calculated as:

$$R = \sqrt{(x_2 - x_1)^2 + (y_2 - y_1)^2 + (z_2 - z_1)^2}.$$

The oblique angle between two vectors in three dimensions was calculated as:

$$\alpha = cos^{-1}[\sin(\theta_1)\sin(\theta_2)\cos(\varphi_1)\cos(\varphi_2) + \sin(\theta_1)\sin(\theta_2)\sin(\varphi_1)\sin(\varphi_2) + \cos(\theta_1)\cos(\theta_2)].$$

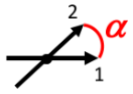

A slip angle θ_s was calculated as:

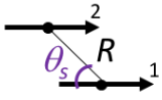

$$\theta_{si} = \cos^{-1}[\boldsymbol{n_i} \cdot \boldsymbol{n_{12}}]$$

Where θ_i and φ_i are the zenith and azimuth angles, in degrees; $\boldsymbol{n_i}$ is a unit orientation vector given by:

$$\boldsymbol{n_i} = \sin(\theta_i)\cos(\varphi_i)\hat{x} + \sin(\theta_i)\sin(\varphi_i)\hat{y} + \cos(\theta_i)\hat{z}$$

And where $\boldsymbol{n_{12}}$ is a unit vector connecting dye centers is:

$$\boldsymbol{n_{12}} = \frac{1}{R_{1,2}}[(x_2 - x_1)\hat{x} + (y_2 - y_1)\hat{y} + (z_2 - z_1)\hat{z}]$$

Extracted $J_{1,2}$ values and calculated geometric parameters for bacteriochlorin dimers are summarized in **Table S7**.

Table S3. KRM monomer parameters for **BC** monomer and **777B**.

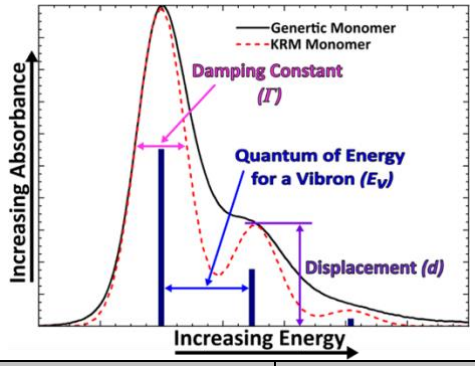

Parameter		[a]BC Monomer	[b]777B
The energy of vibron	E_v,/ *meV*	70.0	165
Displacement of excited state vibronic potential	*d* / dimensionless	0.600	0.709
Energy loss damping constant	*Γ*/ *meV*	21.3	30.0
Characteristic exchange energy	J_0 / *meV•nm*^{3}	16.9	19.9
Electronic Excitation Energies	E_0 / *meV*	1.616	1.599
Transition Dipole moment	*M* /*D*	6.932	7.524
Length of the transition dipole moment ***M***	*l* / *nm*	1.15	0.800
Closest allowed distance between the TMD	*cdis* / *nm*	0.34	0.34

[a]**BC** tethered to DNA in 1× TBE, 15 mM $MgCl_2$. [b]"free" ***Bchla*** in aqueous phosphate buffer.

Table S4. The input fitting parameters used in modeling of **BC** synthetic bacteriochlorin dimer and **820B** natural bacteriochlorin dimer.

Parameter		BC Dimer (Case 1)	BC Dimer (Case 2)	B820 Dimer
Vibrational state Hilbert space	n_v	3	3	3
Energy offset	E_{of} / *meV*	0	0	-50
Closest allowed distance between TMDs of dyes	*cdis* / *nm*	0.34	0.34	0.34

Table S5. The goodness of the fit parameters for absorbance and circular dichroism spectra for **BC** dimer and **820B**.

Construct	***rr***	OI_{AB}	OI_{CD}	OI_{Tot}	MSD_{abs}	MSD_{cd}	$w_{abscd}rms$
BC Dimer (Case 1)	0.995	0.993	0.668	0.831	0.060	2.190	0.060
BC Dimer (Case 2)	0.993	0.987	0.631	0.809	0.130	2.619	0.130
B820 Dimer	1.029	0.959	0.949	0.954	0.377	0.514	0.891

rr - The ratio of theoretical to experimental values of the ratio of the max abs CD peak height to max absorbance peak height
MSD_{abs} - Absorbance spectrum mean-square deviation.
MSD_{cd} - CD spectrum mean-square deviation.
OI_{AB} - Normalized overlap integral for the experimental and theoretical absorbance curves
OI_{CD} - Normalized overlap integral for the experimental and theoretical CD spectra
OI_{Tot} - Mean of OI_{AB} and OI_{CD}
$w_{abscd}rms$ - Weighted mean-squared deviation between the experimental and theoretical absorbance and CD

Table S6. The KRM output of **BC** and **B820** dimer TDM vectors in spherical and Cartesian coordinates.

BC Dimer (Case 1)					
Dye	$\boldsymbol{\theta_i}$ **(°)**	$\boldsymbol{\varphi_i}$ **(°)**	$\boldsymbol{x_i}$ **(nm)**	$\boldsymbol{y_i}$ **(nm)**	$\boldsymbol{z_i}$ **(nm)**
1	137.31	0.00	0.000	0.000	-0.522
2	68.29	-1.47	0.000	0.000	0.522
BC Dimer (Case 2)					
Dye	$\boldsymbol{\theta_i}$ **(°)**	$\boldsymbol{\varphi_i}$ **(°)**	$\boldsymbol{x_i}$ **(nm)**	$\boldsymbol{y_i}$ **(nm)**	$\boldsymbol{z_i}$ **(nm)**
1	82.91	0.00	0.000	0.000	-0.333
2	111.96	-5.76	0.000	0.000	0.333
820B Dimer					
Dye	$\boldsymbol{\theta_i}$ **(°)**	$\boldsymbol{\varphi_i}$ **(°)**	$\boldsymbol{x_i}$ **(nm)**	$\boldsymbol{y_i}$ **(nm)**	$\boldsymbol{z_i}$ **(nm)**
1	7.01	0.00	0.000	0.000	-0.503
2	34.81	4.84	0.000	0.000	0.503

Table S7. Calculated $J_{1,2}$ and geometric parameters of **BC** dimer and **B820** dimer.

Dimer Aggregate	$\boldsymbol{J_{1,2}}$ **(*meV*)**	***R* (Å)**	$\boldsymbol{d_{min}}$ **(*nm*)**	**α (°)**	$\boldsymbol{\theta_{s1}}$ **(°)**	$\boldsymbol{\theta_{s2}}$ **(°)**
BC Dimer (Case 1)	18.5	10.45	0.34	69.03	137.31	68.29
BC Dimer (Case 2)	26.6	6.66	0.34	29.59	97.09	68.04
820B Dimer	35.5	10.06	0.34	27.83	7.01	34.81

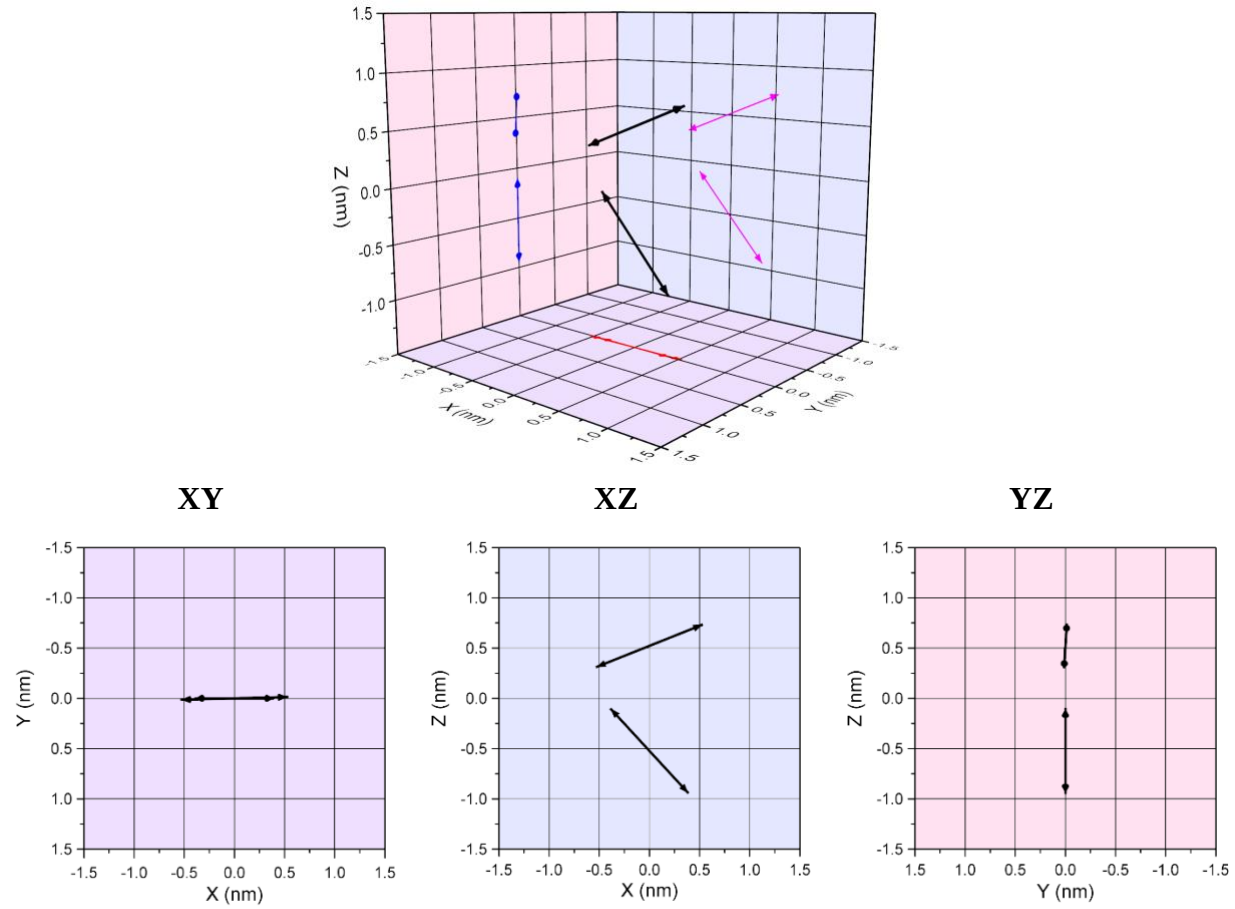

Figure S16. KRM-derived (top) three-dimensional TMD vector plot of **BC** dimer **(Case 1)** and (bottom) TMD plane projections XY, XZ, and YZ.

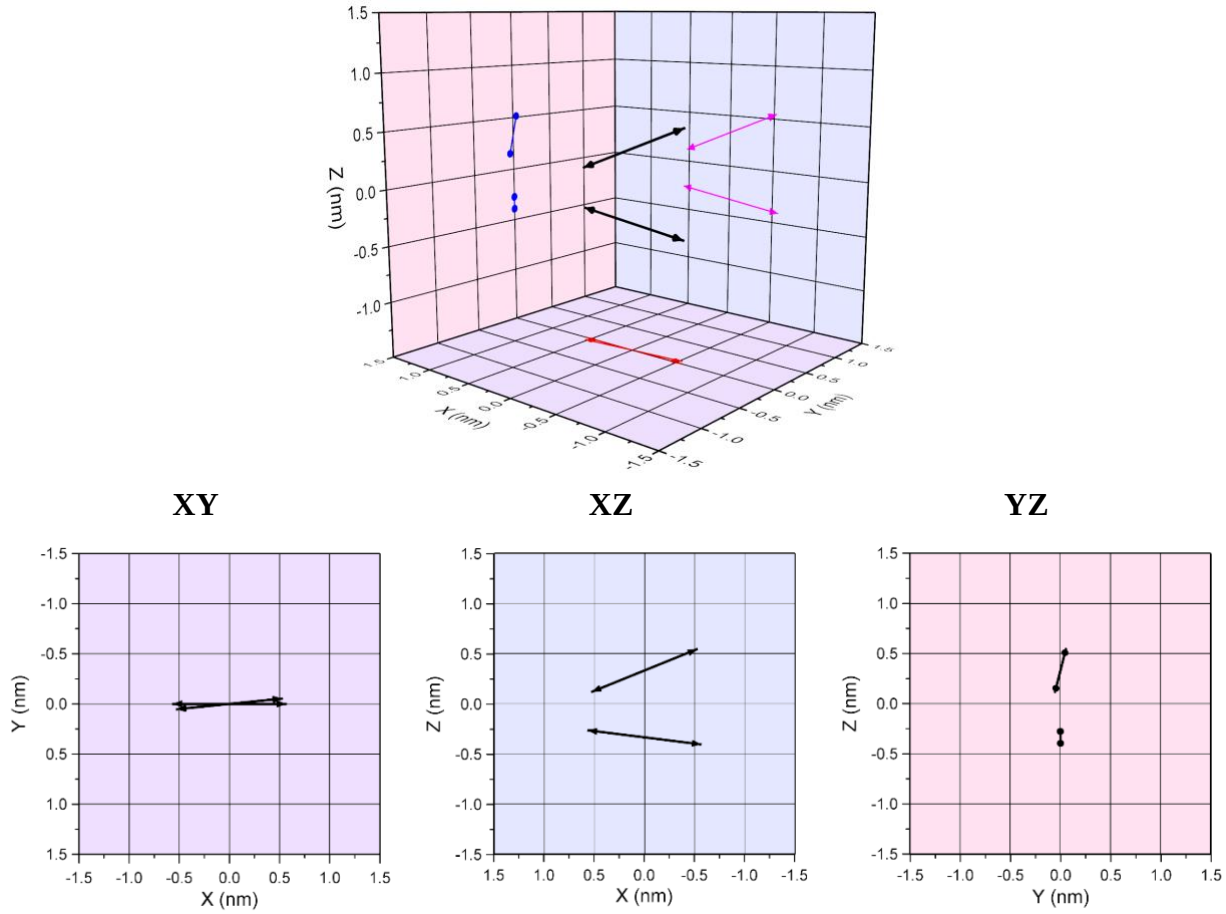

Figure S17. KRM-derived (top) three-dimensional TMD vector plot of **BC** dimer **(Case 2)** and (bottom) TMD plane projections XY, XZ, and YZ.

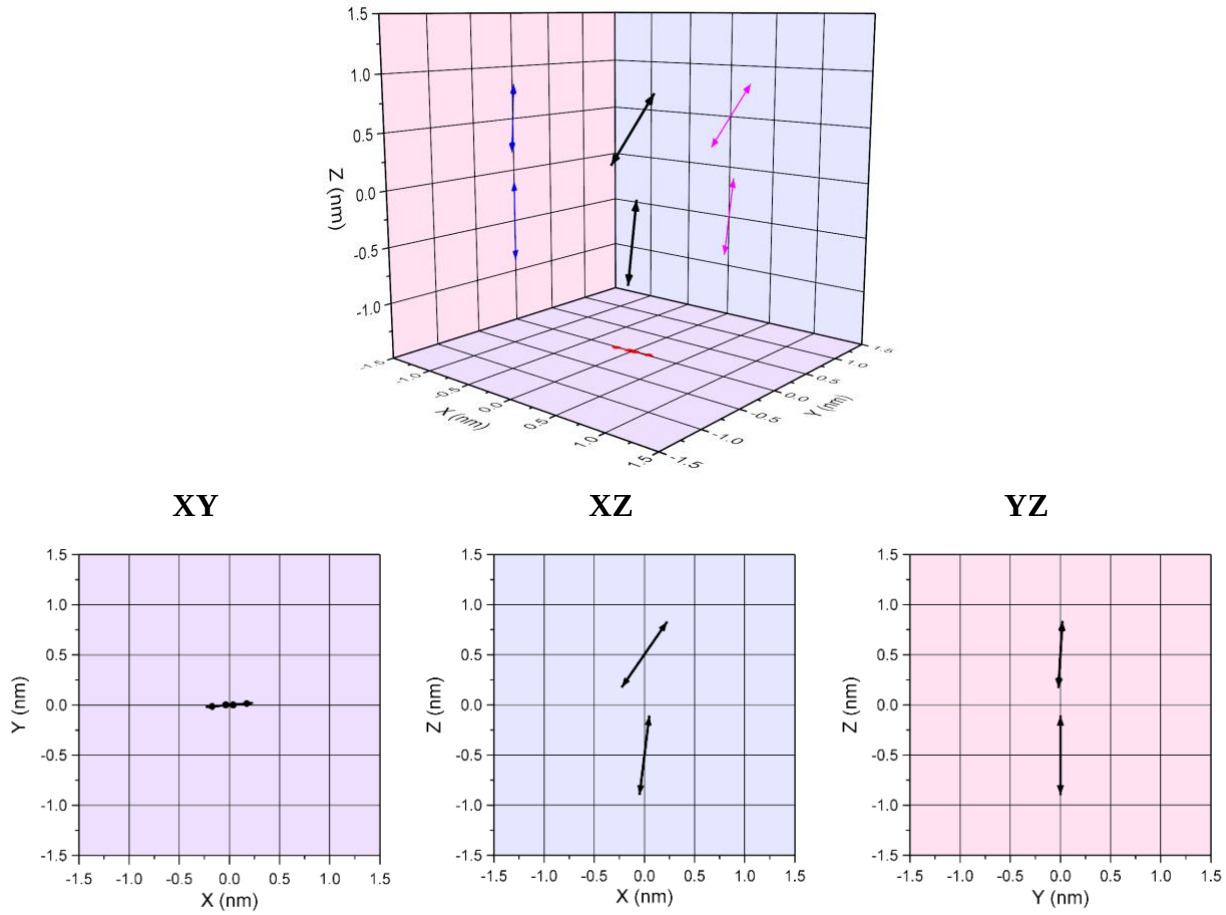

Figure S18. KRM-derived (top) three-dimensional TMD vector plot of **820B** dimer and (bottom) TMD plane projections XY, XZ, and YZ.

Supporting Information 9: *References*

(1) Parkes-Loach, P. S.; Sprinkle, J. R.; Loach, P. A. Reconstitution of the B873 Light-Harvesting Complex of Rhodospirillum Rubrum from the Separately Isolated .Alpha.-And .Beta.-Polypeptides and Bacteriochlorophyll A. *Biochemistry* **1988,** *27*, 2718-2727, DOI:10.1021/bi00408a011.

(2) Rohatgi, A. Webplotdigitizer: Version 4.6. https://automeris.io/WebPlotDigitizer.

(3) Chang, M. C.; Meyer, L.; Loach, P. A. Isolation and Characterization of a Structural Subunit from the Core Light-Harvesting Complex of Rhodobacter Sphaeroides 2.4.1 and Puc705-Ba. *Photochem Photobiol* **1990,** *52*, 873-881, DOI:10.1111/j.1751-1097.1990.tb08696.x.

(4) Roy, S. K.; Mass, O. A.; Kellis, D. L.; Wilson, C. K.; Hall, J. A.; Yurke, B.; Knowlton, W. B. Exciton Delocalization and Scaffold Stability in Bridged Nucleotide-Substituted, DNA Duplex-Templated Cyanine Aggregates. *The Journal of Physical Chemistry B* **2021,** *125*, 13670-13684, DOI:10.1021/acs.jpcb.1c07602.

(5) Holstein, T. Studies of Polaron Motion: Part I. The Molecular-Crystal Model. *Annals of Physics* **1959,** *8*, 325-342.

(6) Abramavicius, D.; Palmieri, B.; Voronine, D. V.; Šanda, F.; Mukamel, S. Coherent Multidimensional Optical Spectroscopy of Excitons in Molecular Aggregates; Quasiparticle Versus Supermolecule Perspectives. *Chemical Reviews* **2009,** *109*, 2350-2408, DOI:10.1021/cr800268n.

(7) Abramavicius, D.; Mukamel, S. Exciton Dynamics in Chromophore Aggregates with Correlated Environment Fluctuations. *The Journal of Chemical Physics* **2011,** *134*, DOI:10.1063/1.3579455.

(8) Abramavicius, D.; Palmieri, B.; Mukamel, S. Extracting Single and Two-Exciton Couplings in Photosynthetic Complexes by Coherent Two-Dimensional Electronic Spectra. *Chemical Physics* **2009,** *357*, 79-84, DOI:http://dx.doi.org/10.1016/j.chemphys.2008.10.010.

(9) Czikklely, V.; Forsterling, H. D.; Kuhn, H. Extended Dipole Model for Aggregates of Dye Molecules. *Chemical Physics Letters* **1970,** *6*, 207-210, DOI:https://doi.org/10.1016/0009-2614(70)80220-2.

(10) Chung, P.-H.; Tregidgo, C.; Suhling, K. Determining a Fluorophore's Transition Dipole Moment from Fluorescence Lifetime Measurements in Solvents of Varying Refractive Index. *Methods and Applications in Fluorescence* **2016,** *4*, 045001, DOI:10.1088/2050-6120/4/4/045001.